Electrochimica Acta 108 (2013) 680–689

Contents lists available at ScienceDirect

Electrochimica Acta

journal homepage: www.elsevier.com/locate/electacta

Layer-by-layer assembled porous CdSe films incorporated with plasmonic gold and improved photoelectrochemical behaviors

Aiping Liu[a,b,*], Qinghua Ren[a], Ming Yuan[a], Tao Xu[a], Manlin Tan[c], Tingyu Zhao[a], Wenjun Dong[a], Weihua Tang[d]

[a] Center for Optoelectronics Materials and Devices, Key Laboratory of Advanced Textile Materials and Manufacturing Technology, Ministry of Education, Zhejiang Sci-Tech University, Hangzhou 310018, China
[b] State Key Lab of Silicon Materials, Zhejiang University, Hangzhou 310027, China
[c] Low Carbon Energy & Energy Saving Laboratory, Research Institute of Tsinghua University in Shenzhen, Shenzhen 518057, China
[d] State Key Laboratory of Information Photonics and Optical Communication, Beijing University of Posts and Telecommunications, Beijing 100876, China

ARTICLE INFO

Article history:
Received 26 January 2013
Received in revised form 2 July 2013
Accepted 2 July 2013
Available online 13 July 2013

Keywords:
Metallic plasmon
Porous CdSe film
Multilayer strucuture
Photoelectrochemical behavior
Solar cells

ABSTRACT

A simple method for creating three-dimensional porous wurtzite CdSe films incorporated with plasmonic gold by the electrochemical layer-by-layer assembly was proposed. A prominent enhancement in light absorption of CdSe films was attained by the efficient light scattering of gold plasmons as sub-wavelength antennas and concentrators and the near-field coupling of gold plasmons with the neighboring porous CdSe films. The broadband photocurrent enhancement of Au–CdSe composite systems in the visible light range and the local current maximum between 600 and 700 nm suggested the cooperative action of antenna effects and electromagnetic field enhancement resulting from localized surface plasmon excitation of gold. Furthermore, the photoelectrochemical response of porous Au–CdSe composite films was highly tunable with respect to the number of Au–CdSe bilayer. The optimal short-circuit current and open-circuit potential were obtained in a four-layer Au–CdSe system because the thicker absorber layer with less porous structure might limit the electrolyte diffusion into the hybrid electrode and impose a barrier for electron tunneling and transferring. The highly versatile and tunable properties of assembled porous Au–CdSe composite films demonstrated their potential application in energy conversion devices.

1. Introduction

Consideration for the employment of unlimited, clear and environmentally friendly new energy, photovoltaic cells specially thin-film solar cells have been given great attention because of the comparatively low material and processing costs [1]. However, the low energy conversion efficiency of such cells is still a primary challenge for the large-scale application of thin-film solar cells. An effective method for enhancing light harvesting or trapping to develop high-efficiency thin-film photovoltaic devices is the mergence of metallic nanostructures with high absorption and scattering cross section [2,3] which concentrate sunlight into the semiconductor absorber layer, thereby permitting a considerable reduction in the physical thickness of photovoltaic absorber layers [4]. The local near-field enhancement in the proximity of metal nanostructures, which is associated with the surface plasmon (SP) excitation induced by visible light irradiation, can also favor carrier generation and separation and increase photocurrents when the metallic plasmons couple with the neighboring photovoltaic absorber layers and transfer the plasmonic energy from the metal to the semiconductor [5,6]. Since the plasmon resonance energy strongly depends on the metal particle size and shape, interparticle spacing, and dielectric property of the surrounding medium [7–11], it is available to improve the photoelectric activity of the semiconductor by designing and synthesizing targeted metal nanoparticles (NPs) or nanostructures, indicating the potential application of metallic plasmons in optoelectronic and photonic devices [1,4,9,11–24], photocatalysts [6,25–29] and sensors [30–34]. The recent advances in control of metal NP synthesis and self-assembly have successfully tailored high absorption of absorber layers throughout the visible region to the near infrared one by varying metal size and shape [35,36]. The distance needed for the coupling effect between the approached gold NPs has been adjusted by the thickness of middle semiconductor nanosheets [28]. The "hot spot" between the nearly touching metal NPs

* Corresponding author at: Center for Optoelectronics Materials and Devices, Key Laboratory of Advanced Textile Materials and Manufacturing Technology, Ministry of Education, Zhejiang Sci-Tech University, Hangzhou 310018, China.
Tel.: +86 571 86843468; fax: +86 571 86843468.
E-mail address: liuaiping1979@gmail.com (A. Liu).

0013-4686/$ – see front matter © 2013 Elsevier Ltd. All rights reserved.
http://dx.doi.org/10.1016/j.electacta.2013.07.019

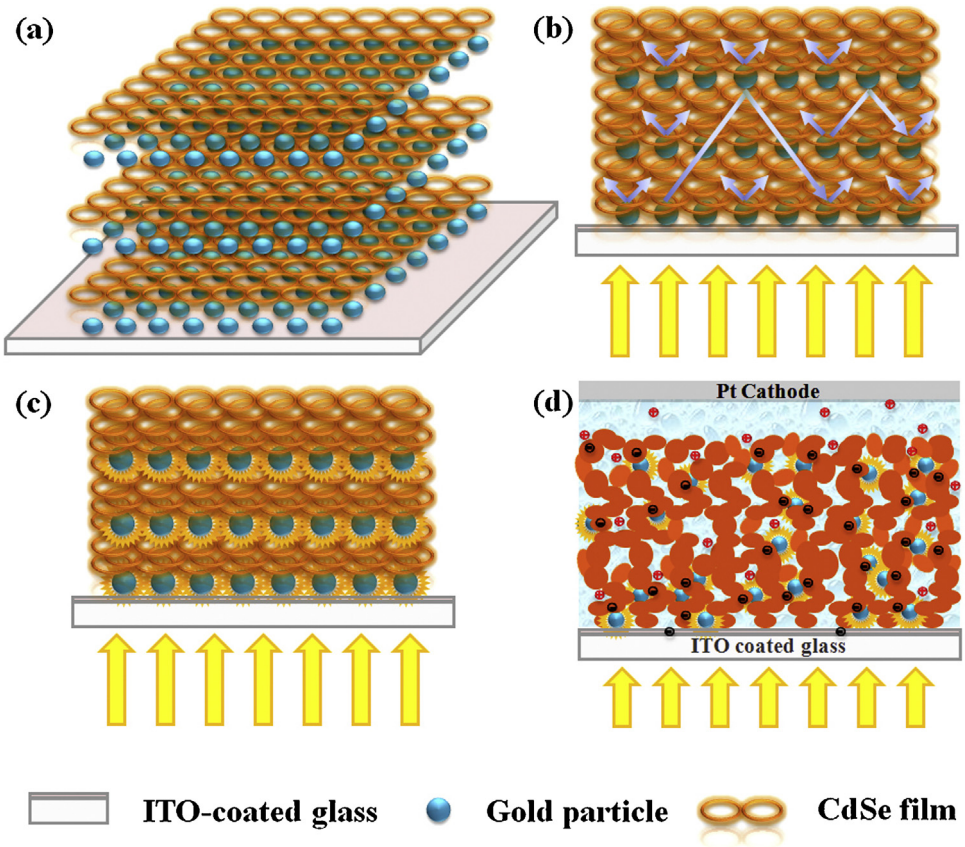

Fig. 1. (a) Schematic representation of layer-by-layer assembled $(Au–CdSe)_n$ film, (n is the number of Au–CdSe bilayer, typically $n = 1–5$). Light trapping and concentration by (b) the scattering from gold nanoparticles and (c) the excitation of localized surface plasmons in gold nanoparticles embedded in the CdSe semiconductor. (d) Illustration of charge separation in the CdSe semiconductor induced by the concentrated resonance energy contained in localized plasmonic oscillations for the thin-film solar cell with the porous $(Au–CdSe)_n$ film as the photoanode.

has induced several orders of magnitude enhancement of local field effect in comparison with those isolated metal NPs [37]. However, among the numerous fabrication techniques for precise control of reproducible metallic plasmons, the surfactant dosages, reaction rate and temperature need be accurately controlled in chemical reaction process and the resultant metallic nanostructures must be separated from heterogeneous impurities before use. The lithography techniques are used restrictedly considering the throughput and cost, and suitable to pattern only small areas. The electrodeposition with simple, rapid and low-cost properties can produce well-defined metallic nanostructures with SP-active nature and is regarded to be practical for mass production [32,38,39].

In this paper, we fabricate three-dimensional porous CdSe films mergenced with the plasmonic gold by alternating layer-by-layer assembly in a simple electrodeposition process, as shown schematically in Fig. 1(a). The gold nanostructures electrodeposited on the conductive ITO-coated glass surfaces are used as conducting scaffolds to anchor active CdSe semiconductor for light harvesting. The plasmonic gold nanostructures can be expected as the scattering elements to couple and trap the sunlight into the CdSe absorber film and locally amplify the electromagnetic field when placed on the surface or inside the CdSe [4], increasing the effective absorption cross-section and optical path length inside the absorber (Fig. 1b). Furthermore, the concentrated resonance energy contained in localized plasmonic oscillations (Fig. 1c) can be transferred to the semiconductor, inducing charge separation in the semiconductor (Fig. 1d) [5]. By the alternating assembly of plasmonic gold nanostructures and porous CdSe films, we have succeeded in developing a novel multilayered photovoltaic material with adjustable light absorption and photovoltaic response.

2. Experimental

2.1. Reagents

The ITO-coated glasses (1.5 cm × 2.5 cm) with the sheet resistance of 8 Ω/sq. and $HAuCl_4·3H_2O$ with a purity of 99.99% were supplied by Sigma. All other chemicals were of analytical grade and used without further purification. The water was obtained from a Millipore Q purification system (resistivity >18 MΩ cm).

2.2. Preparation of multilayered Au–CdSe composite films

The ITO-coated glasses were cleaned ultrasonically with soapy water, acetone, ethanol and distilled water, respectively, and dried with N_2 before use. The ITO-coated glass was successively immersed into a 1 M Na_2SO_4 solution containing 2 mM $HAuCl_4$ to electrodeposit gold NPs on the ITO surfaces at −0.8 V (*vs.* saturated calomel electrode, SCE) for 20 s, 50 s, 100 s, 300 s and 600 s, respectively. An electrochemical workstation (CHI 630D, USA) with the ITO working electrode, SCE reference electrode and platinum foil counter electrode was used. After the gold nanostructured ITO substrates were dried with N_2, the CdSe semiconductor films were electrodeposited on the plasmonic gold surfaces from aqueous plating solutions (pH 6.0) containing 0.25 M $CdSO_4$, 0.25 M Na_2SO_4 and 14 mM SeO_2 at ambient temperature using a cyclic voltammetry

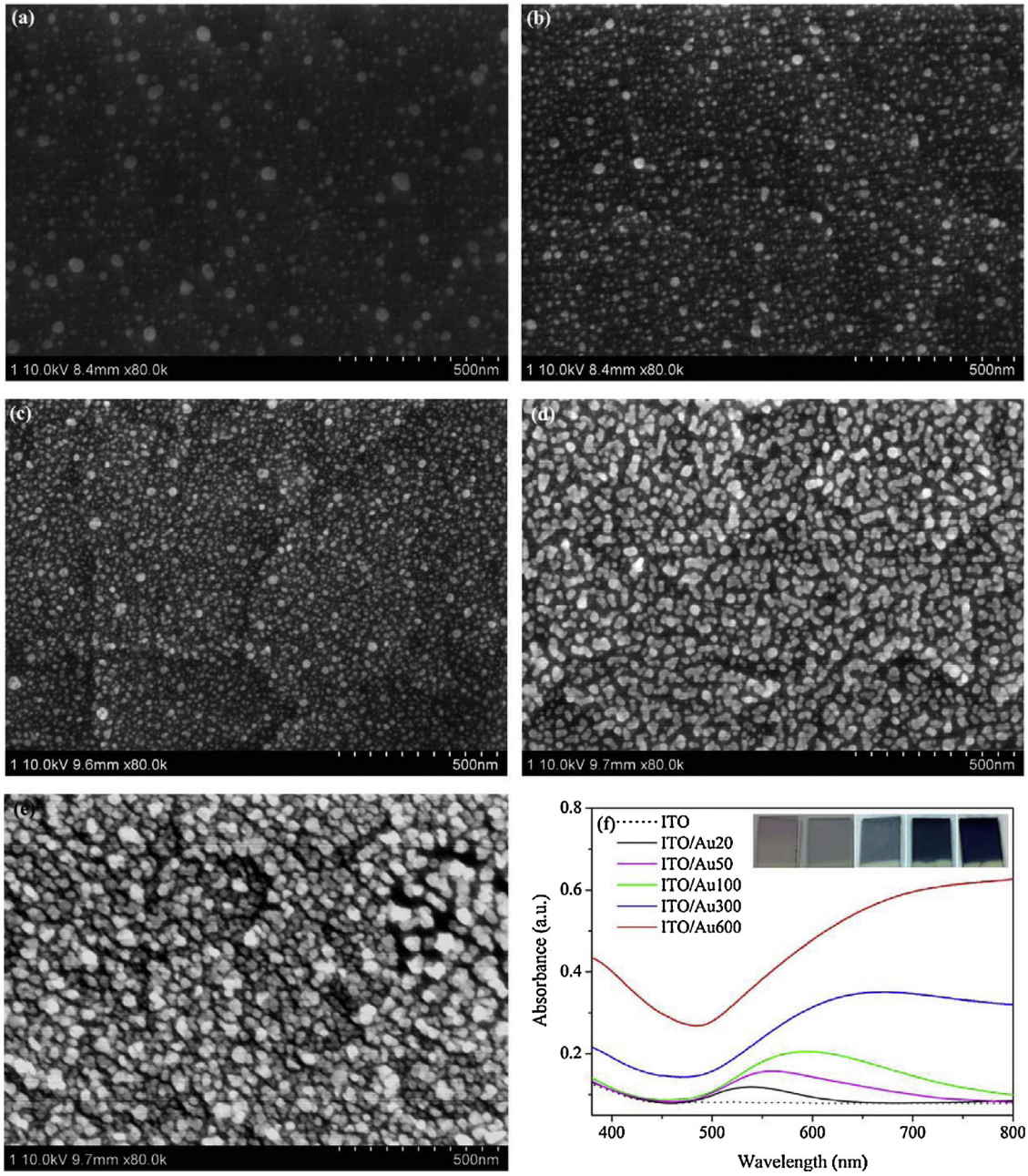

Fig. 2. Scanning electron micrographs of gold plasmons electrodeposited on ITO-coated glass substrates for (a) 20 s, (b) 50 s, (c) 100 s, (d) 300 s and (e) 600 s, respectively, in a 1 M Na_2SO_4 solution containing 2 mM $HAuCl_4$. (f) UV–vis absorption spectra and photographs of ITO/Au samples prepared at different electrodeposition times.

technique with the sweep potential between −0.35 V and −0.75 V *vs*. SCE at a sweep rate of 30 mV/s for 2, 4, 9 and 18 min. The resultant ITO/Au–CdSe electrodes were washed with deionized water, dried with N_2 and annealed at nitrogen atmosphere at 400 °C for 1 h. Repeating the plasmonic gold and CdSe film electrodeposition processes alternately, the porous Au–CdSe composite structures were obtained with the samples labeled as ITO/$(Au–CdSe)_n$ (n was the number of Au–CdSe bilayer, which was changed from 1 to 5). The sample that the CdSe film was directly deposited on ITO surface without the plasmonic gold assemblies was prepared as a control.

2.3. Characterization and measurements

The morphologies and compositions of Au–CdSe composite films were obtained by a scanning electron microscopy (SEM) instrument (Hitachi S-4800, Japan) equipped with an energy-dispersive X-ray spectroscopy (EDS). X-ray diffraction (XRD) patterns of composite films were obtained on a diffractometer (Bruker AXS D8) using the CuK_α radiation (λ = 0.15418 nm) with a 2θ scan from 5° to 80° at a step of 0.02°. The UV–vis absorption spectra of composite films on ITO substrates were recorded by using a Thermo Electron UV–vis spectrophotometer (UV-2400PC, Shimadzu, Japan). The Raman spectra were acquired with a Thermo Fisher DXR Raman spectrometer using a He–Ne laser (λ = 514.5 nm).

Photoelectrochemical performances of composite films were measured in a transparent quartz cell with the 0.2 M Na_2S aqueous solution as the electrolyte. Two-electrode system was used with the porous Au–CdSe film as the working electrode and a platinum foil as the counter electrode. The curves of photovoltage and photocurrent *vs.* times under white light irradiation were recorded by the electrochemical workstation (CHI 630D, USA) using a 150 W Xenon lamp (λ > 300 nm) as the light source. The wavelength

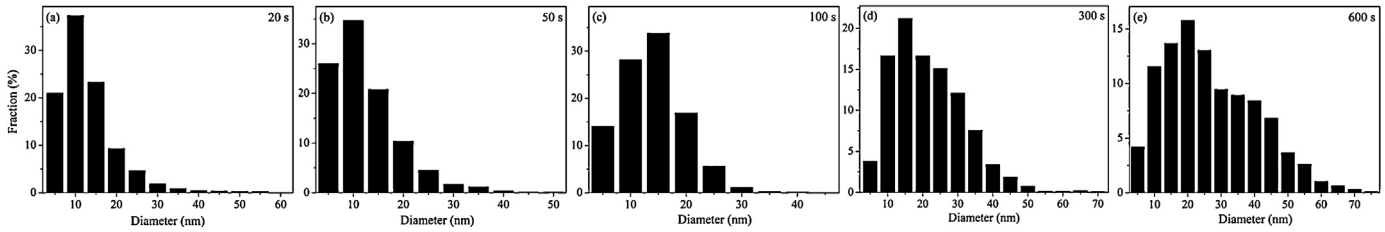

Fig. 3. Particle size distributions of (a) ITO/Au20, (b) ITO/Au50, (c) ITO/Au100, (d) ITO/Au300 and (e) ITO/Au600 samples prepared at different electrodeposition times.

dependent photocurrent response was tested by the UV–vis Xenon lamp with a motorized monochromator (Kratos), which allowed monochromatic irradiation of the specimen surface through the electrochemical cell quartz window. The illumination intensity of white light near the electrode surface was about 100 mW/cm^2. All measurements were carried out in air at room temperature.

3. Results and discussion

3.1. Microstructures of Au–CdSe bilayers

The morphologies of typical gold NPs electrodeposited on the ITO substrates are shown in Fig. 2. The gold NPs after 20 s deposition (Au20) present a broad particle size distribution from 2.1 nm to 57.8 nm with an average diameter about 11.8 nm (Figs. 2a and 3a). With the increase of deposition time to 50 s and 100 s, the gold NPs are more concentrated and homogeneous (the particle size distribution from 2.4 nm to 47.8 nm for Au50 and from 2.7 nm to 39.9 nm for Au100) (Figs. 2b, c and 3b, c). The average diameters are about 12.6 nm for Au50 and 14.3 nm for Au100, respectively. This indicates that the gold nucleation on ITO substrate agrees well with the progressive nucleation mechanism, namely new gold nuclei may be continuously formed at a vacant position of ITO surface [40], which decreases the distance between gold NPs. Further lengthening the electrodeposition time, the gold grows irregularly (Fig. 2d) and forms denser multilayered particle film after 600 s (Fig. 2e). The average diameters are about 22.6 nm for Au300 with the particle size distribution from 2.8 nm to 69.4 nm, and 26.1 nm for Au600 with the particle size distribution from 2.9 nm to 74.8 nm, respectively. The absorption peak of plasmon mode of gold NPs (Au20) on the ITO substrate (Fig. 2f) is similar to that of gold NPs in an aqueous environment (centered at about 525 nm) [41,42], but with a redshift by about 14 nm due to the increase in refractive index of environment (from water to ITO-coated glass) and plasmon coupling between gold NPs [43]. The longer tails of the absorption peaks for Au100 and Au300 suggest a significant getting closer and aggregated gold NPs with each other [36]. The aspect ratio of the irregular aggregations for Au300 might be close to the order of 2:1 when considering an absorption peak of SP mode over 600 nm [36,44]. The redshift of absorption peak may also be associated with the electromagnetic field enhancement around the gold NPs [36,45,46], as theoretically predicted for the localized surface plasmon resonance (LSPR) of gold [47]. Upon lengthening the deposition time to 600 s, the absorption peak undergoes a significant redshift over 700 nm, accompanying the dramatic increase in the absorption intensity due to the formation of denser and aggregated particle films with deeper color (Fig. 2f).

Fig. 4 displays the cyclic voltammogram of CdSe deposition on the ITO/Au surface, which is related to the formation of H_2SeO_3 in the weak acidic solution, the reduction of SeO_3^{2-} to elemental selenium or to Se^{2+} (Eqs. (1)–(3)) and the reduction of CdSe in the presence of cadmium ions (Eq. (4)) [48–50]. When the applied potential is scanned to about −0.40 V, a slightly visible golden film appears on the electrode surface, which is attributed to the reduction of SeO_3^{2-} (Eq. (2)). The color of film becomes deeper when the applied potential increases to about −0.65 V, indicating the reduction of CdSe (Eq. (4)). With the cathodic potential changes more negative (<−0.8 V), the electrochemical reduction of cadmium ion to elemental cadmium will occur (Eq. (5)), followed by the stripping of the metallic cadmium phase in the positive scan (at about −0.4 V) [51,52]. Since no electrochemical anodic process related to cadmium oxidation can be seen in our experiment, this demonstrates the suppression of cadmium ion reduction in our potential range from −0.35 V to −0.75 V in order to achieve stoichiometric 1:1 CdSe semiconductor.

$$SeO_2 + H_2O \rightarrow H_2SeO_3, \quad (1)$$

$$SeO_3^{2-} + 6H^+ + 4e^- \rightarrow Se^0 + 3H_2O, \quad (2)$$

$$Se^0 + 2e^- \rightarrow Se^{2-}, \quad (3)$$

$$H_2Se + Cd^{2+} \rightarrow CdSe + 2H^+, \quad (4)$$

$$Cd^{2+} + 2e^- \rightarrow Cd. \quad (5)$$

The resultant CdSe film on ITO-coated glass substrate after 9-min electrodepositon shows a homogeneous ordered porous structure with a pore diameter about 50–70 nm (Fig. 5a). The CdSe film deposited on gold coated ITO substrate possesses an analogous ordered porous structure with a broader pore size distribution (Fig. 5b–f). Smaller and fewer pores can be found with the increasing deposition time of gold NPs (Fig. 5f), indicating the CdSe film getting denser. The thickness of CdSe films changes from ~45 nm on ITO/Au20 to ~100 nm on ITO/Au300 and to ~140 nm on ITO/Au600 compared to the 110 nm for the CdSe film directed deposited on the ITO substrate. This indicates that the plasmonic gold appropriately reduces the physical thickness of photovoltaic absorber layer. The EDS result confirms CdSe

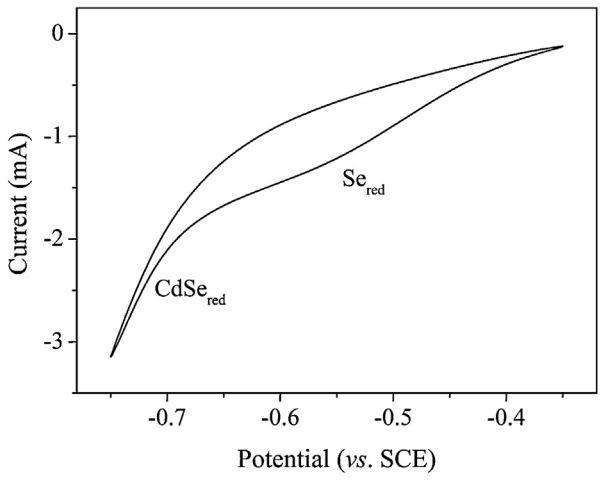

Fig. 4. Cyclic voltammogram of CdSe electrodeposition on the ITO/Au surface in the aqueous plating solutions (pH 6.0) containing 0.25 M $CdSO_4$, 0.25 M Na_2SO_4 and 14 mM SeO_2 at a sweep rate of 30 mV/s.

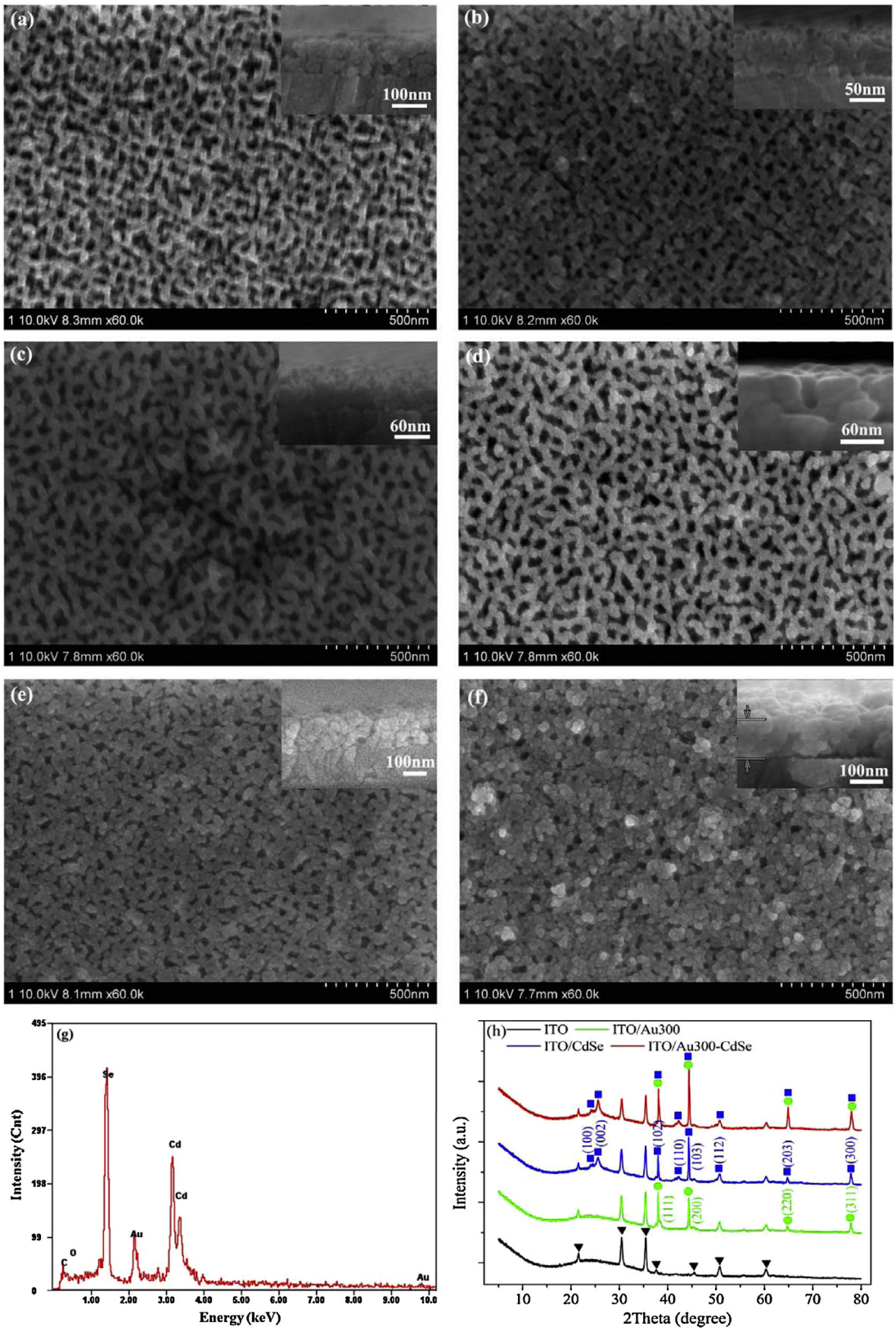

Fig. 5. Scanning electron microscopy images of (a) ITO/CdSe, (b) ITO/Au20–CdSe, (c) ITO/Au50–CdSe, (d) ITO/Au100–CdSe, (e) ITO/Au300–CdSe and (f) ITO/Au600–CdSe samples. The insets are the corresponding cross section images. (g) Energy-dispersive X-ray spectroscopy of ITO/Au300–CdSe film. (h) X-ray diffraction patterns of different samples. The electrodeposition time of all CdSe films was 9 min.

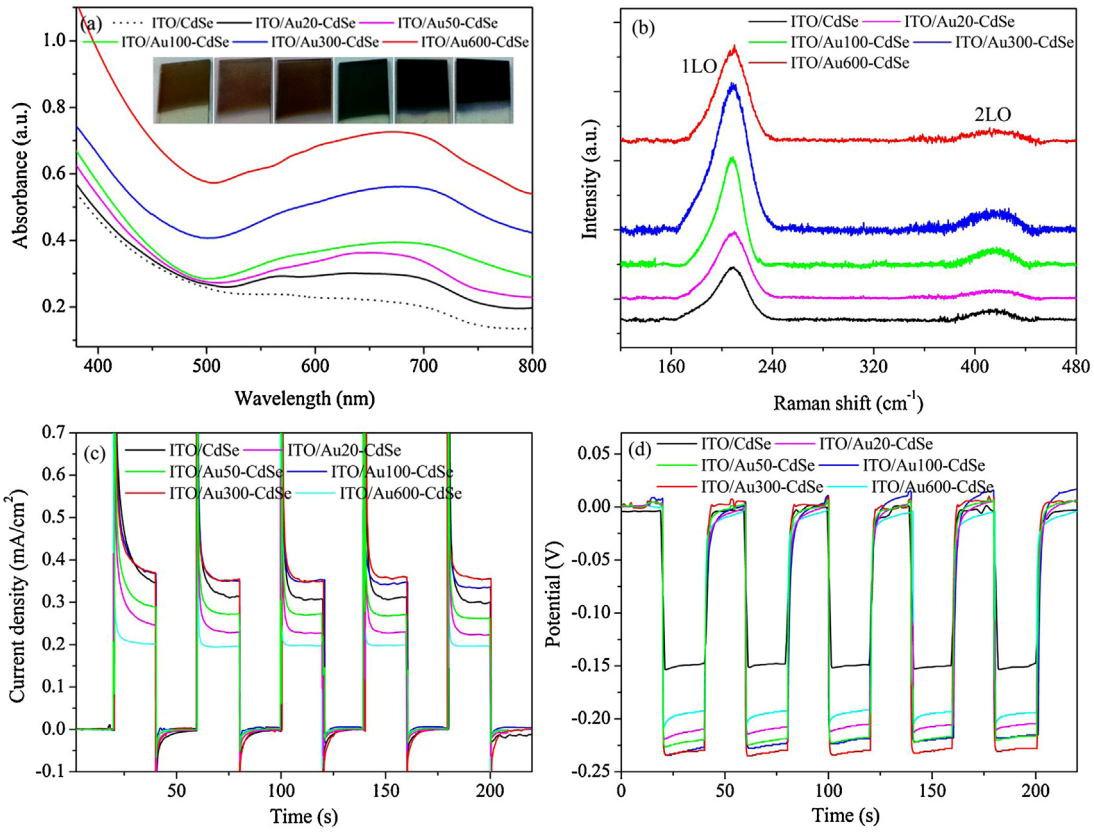

Fig. 6. (a) Photographs and UV–vis absorption spectra, (b) Raman spectra, (c) photocurrent density and (d) open-circuit voltage of ITO/CdSe and ITO/Au–CdSe composites. The electrodeposition time of all CdSe films was 9 min.

presence in the composites with the average atomic percentage of Cd:Se to be 1:1.07 (Fig. 5g). The slightly excess selenium is related to the reduction of SeO_3^{2-} to elemental selenium (Eq. (2)), which is in good agreement with the previous reports [53,54]. However, the mechanism of obtaining the porous CdSe film is unclear, which is independent of the gold existence. A possible explanation is that the weak acidic condition (pH 6.0) might make the formation of Se^0 sites on the electrode surface slowly, resulting in homogeneous growth of CdSe NPs along the grain boundaries of ITO or gold nanocrystals. The SEM images (Fig. 5) show that the porous CdSe films are assembled by a series of CdSe NPs. The XRD patterns in Fig. 5(h) reveal that the peaks appearing at (2θ) 38.0°, 44.3°, 64.6° and 77.8° for gold are corresponding to the (1 1 1), (2 0 0), (2 2 0) and (3 1 1) planes of the face-centered cubic gold [32], and the peaks at (2θ) 23.9°, 25.4° and 42.0° for CdSe film correspond to the (1 0 0), (0 0 2) and (1 1 0) planes of hexagonal wurtzite-type CdSe structure (JCPDF: 08-0459) [55].

3.2. Photoelectrochemical behaviors of Au–CdSe bilayers

Fig. 6(a) shows the photographs of CdSe films after 9-min deposition on different substrates. The ITO/Au–CdSe samples present deeper color compared to the ITO/CdSe due to the influence of gold NPs film. The absorption peaks for ITO/CdSe at 580 nm and 485 nm are assigned to the first and second excitonic transitions of the particles with smaller sizes, and the peak at 698 nm is attributed

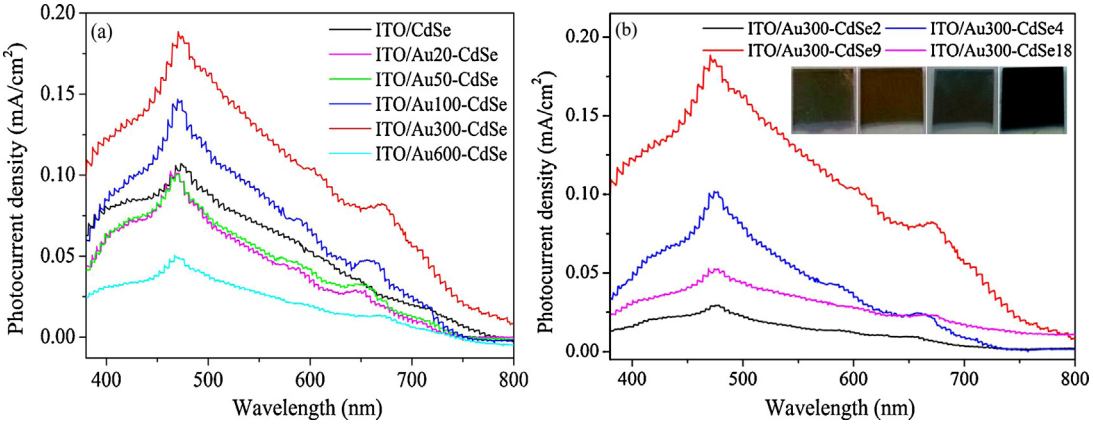

Fig. 7. (a) Wavelength dependent photocurrent response of ITO/CdSe and ITO/Au–CdSe systems. The electrodeposition time of CdSe films was 9 min. (b) Wavelength dependent photocurrent response of ITO/Au300–CdSe systems with CdSe electrodeposited for different times.

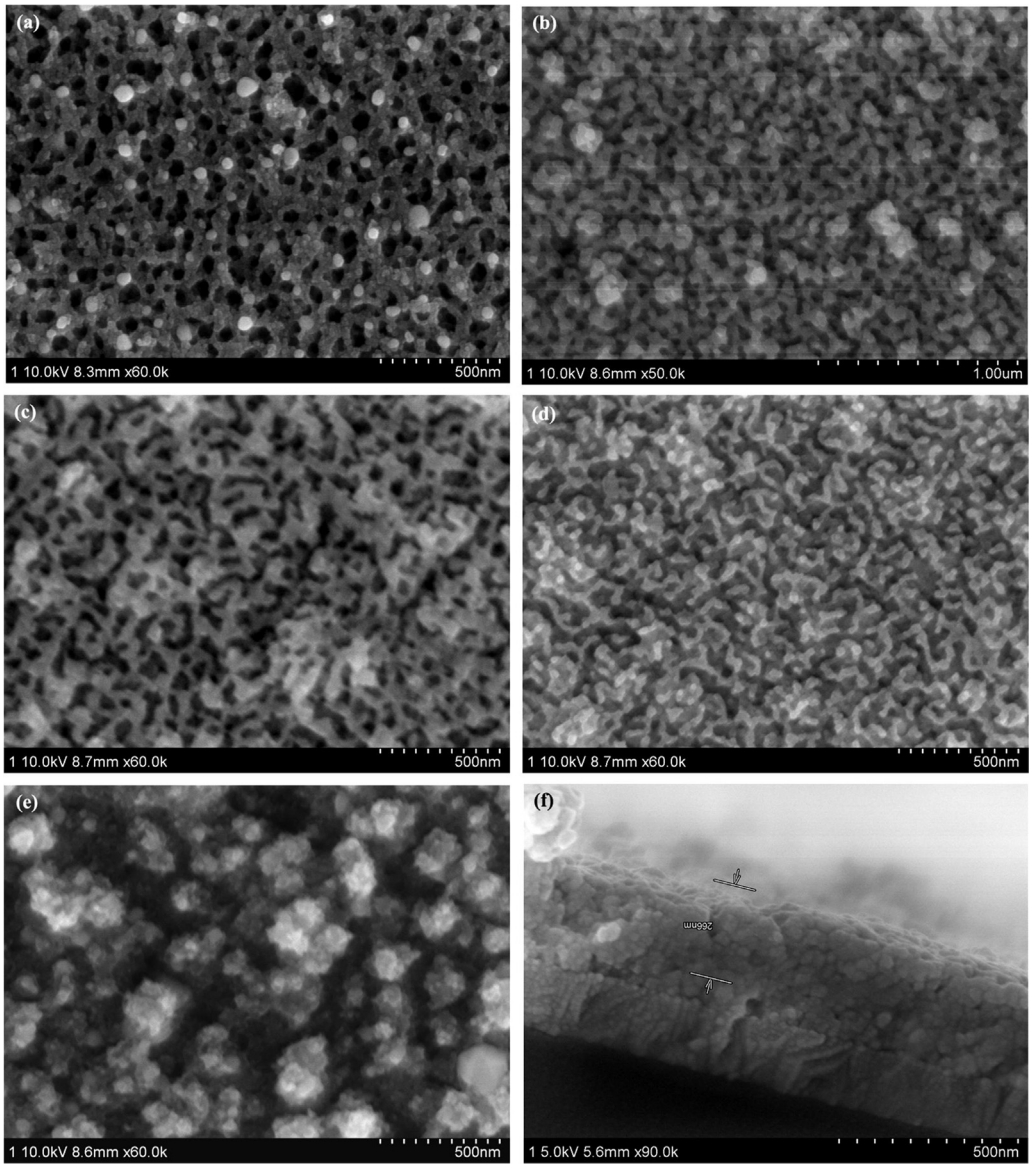

Fig. 8. Scanning electron microscopy images of (a) ITO/(Au–CdSe)$_1$ after secondary gold electrodeposition, (b) ITO/(Au–CdSe)$_2$, (c) ITO/(Au–CdSe)$_3$, (d) ITO/(Au–CdSe)$_4$, (e) ITO/(Au–CdSe)$_5$ and (f) cross section of ITO/(Au–CdSe)$_4$. The electrodeposition times of gold and CdSe monolayers were 300 s and 9 min, respectively.

to the interband transition of the particles with larger sizes [56]. The broadening absorption peak is attributed to the broad particle size distribution in CdSe films. The significant enhancement in absorbance of the CdSe layer with plasmonic gold NPs in the range from 500 nm to 800 nm is attributed to absorption and scattering of plasmonic gold [57]. The light might be preferentially scattered and trapped into the CdSe film by multiple and high-angle scattering on the surface of gold NPs as sub-wavelength scattering elements, causing an increase of effective optical path length in the cell (Fig. 1b) [2]. This reduces the physical thickness of absorber layers in ITO/Au20–CdSe, ITO/Au50–CdSe, ITO/Au100–CdSe and ITO/Au300–CdSe (Fig. 5) while keeping high optical response compared to ITO/CdSe (Fig. 6a) [4]. Furthermore, plasmonics gold NPs with their effective dipole moment located close to the CdSe layer could favor the strong local field enhancement around the gold NPs and near-field coupling with the CdSe semiconductor [58,59] (Fig. 1c), increasing the absorption of semiconductor surrounding and cross-section [60,61]. The plasmonic near-field coupling is usually remarkable for small metallic particles (5–20 nm in diameter) due to their low albedo (fraction of light emitted as radiation) and depends on the metal particle size and shape, interparticle spacing, and dielectric property of the surrounding medium [7–11]. The "hot spot" between the nearly metal NPs is favorable for the great enhancement of local field effect in comparison with those isolated metal NPs [37]. This can be deduced from the Raman spectra of composites with metallic plasmons since the Raman scattering intensity is proportional to the local electric field intensity [62]. In can be seen from the typical Raman scattering spectrum of CdSe (Fig. 6b) that the peaks at about 208 cm^{-1} and 413 cm^{-1} are attributed to the first-order longitudinal optical phonon mode (1LO) and second-order overtone mode (2LO) of wurtzite CdSe, respectively [63]. The increase in Raman intensity of CdSe with gold plasmons compared to the single CdSe is the result of stronger electric field induced by gold NPs under laser excitation. The ITO/Au300–CdSe has a stronger Raman signal than ITO/Au20–CdSe and ITO/Au100–CdSe because of its smaller interparticle spacing. Further increasing the sizes of gold clusters decreases the intensity of characteristic Raman peak of ITO/Au600–CdSe due to the reductive "hot spots" for gold. Besides the improving light absorption of CdSe, the facilitating formation of electron–hole pairs in

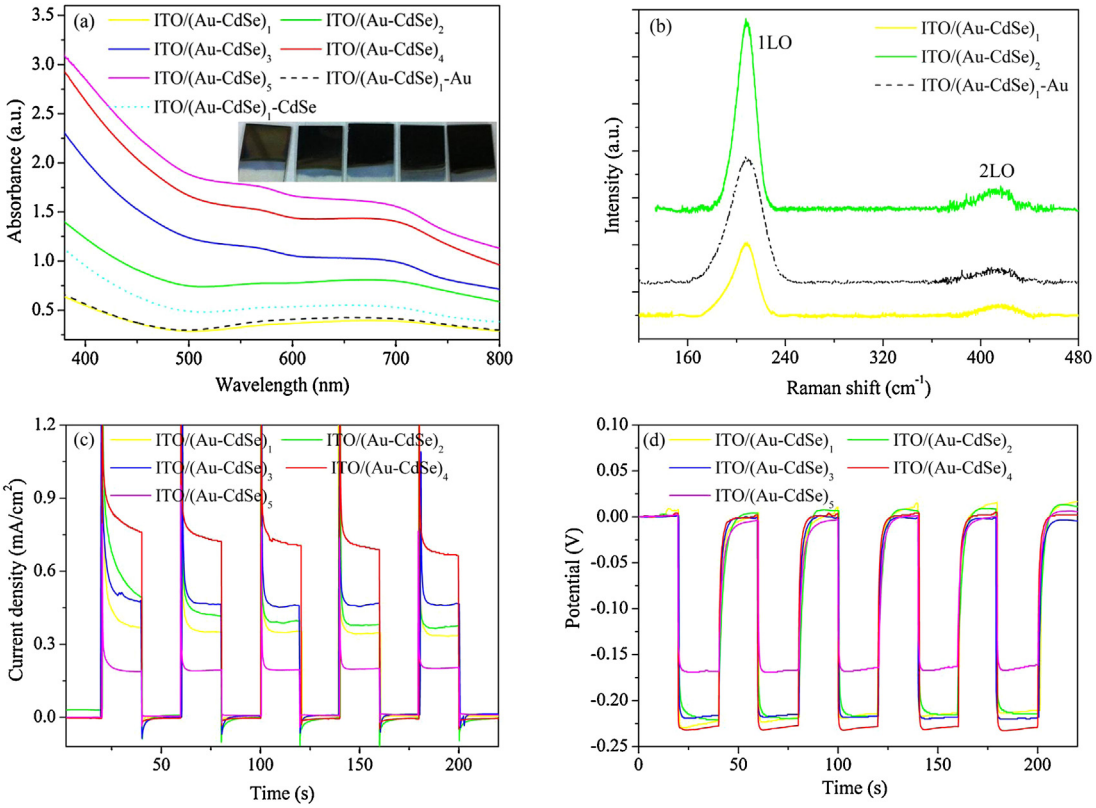

Fig. 9. (a) UV–vis absorption spectra and photographs, (b) Raman spectra, (c) photocurrent density and (d) open-circuit voltage of ITO/(Au–CdSe)$_n$ composite systems (n is the number of Au–CdSe bilayer, typically n = 1–5). The electrodeposition times of gold and CdSe monolayers were 300 s and 9 min, respectively.

the near-surface region of CdSe by the LSPR effect of metal NPs has been broadly reported [6,25,26], resulting in the enhancement of photocurrents [60,64]. Our results have confirmed the obvious enlargement of photocurrent signal for ITO/Au–CdSe systems upon visible white light irradiation (Fig. 6c) by constructing a photoelectrochemical cell system with the platinum foil as a counter electrode and 0.2 M Na_2S aqueous solution as the electrolyte. The lower photocurrent responses of ITO/Au20–CdSe and ITO/Au50–CdSe systems compared to the ITO/CdSe are ascribed to the fewer photogenerated carriers provided by the thinner CdSe films on the gold NPs surfaces. The superior photoelectrochemical properties achieved for the ITO/Au100–CdSe and ITO/Au300–CdSe systems might be attributed to the more electron–hole pairs in the near-surface region of CdSe under the action of concentrated resonance energy and the improved localized electric field of CdSe induced by the SPR effect of neighboring gold NPs (Fig. 1d) [6,25,26]. The intensity of localized electric field is weakened with the reduced "hot spots" when the gold NPs greatly overlap. The CdSe particles in the thicker CdSe film for the ITO/Au600–CdSe system might serve as the recombination centers of the photogenerated holes and electrons and could not transit all electrons to the ITO anode, resulting in the dramatic drop in the short-circuit current response. Takahashi et al. also observed a photocurrent decrement in the dense-packed gold NPs system because of the quenching effects [18,65]. Furthermore, reducing the CdSe thickness by incorporating the plasmonic gold also might improve the electrical characteristics of the solar cell due to the dark current reduction, causing the open-circuit voltage increase (Fig. 6d) [4]. The thickness decrease might also limit surface recombination occurrence because carriers need to travel only a small distance before being collected, leading to a higher photocurrent.

To further confirm the remarkable broadband scattering enhancement of plasmonic gold, wavelength dependent photocurrent response is presented in Fig. 7. The broadband photocurrent enhancement of CdSe with the integration of gold NPs in the visible light range (Fig. 7a) indicates that the large angle scattered light from the gold NPs is trapped inside the CdSe layer. Furthermore, the significant current enhancement between 630 nm and 700 nm with local maximum values might be attributed to the more electron–hole pairs in the near-surface region of CdSe induced by LSP excitation of gold NPs [6,25,26], resulting in the enhancement of the photocurrent near the LSP band [60,64]. The local current enhanced region presents a slight redshift with the size increase of gold NPs and the decrease of interparticle spacing, which is consistent with the changing tendency of absorption band of plasmonic gold (Fig. 2f). This result suggests that the photocurrent enhancement is induced not only by antenna effects but also by electromagnetic field enhancement resulting from the LSP excitation of gold. Additionally, the appropriate increase of CdSe thickness (from about 30 nm to 100 nm) on the Au300 surface also results in the enhancement of photocurrent response in the visible light range (Fig. 7b) because the photogenerated carriers would have trouble in traveling a thicker CdSe film before being collected.

3.3. *Photoelectrochemical behaviors of multilayered Au–CdSe composite systems*

In order to improve the photocurrents, we design multilayered Au–CdSe structure by electrochemical layer-by-layer assembly. As shown in Fig. 8(a), the secondary gold NPs tend to grow on the surface of porous CdSe film of previous Au–CdSe bilayer. The porous structure remains unchanged for ITO/(Au–CdSe)$_2$ and ITO/(Au–CdSe)$_3$ systems. The porous density obviously decreases when the number of bilayer increases to 4 and 5, resulting in a denser CdSe film (Fig. 8f). The successful growth of multilayers is monitored by the gradual increase of characteristic SP absorbance

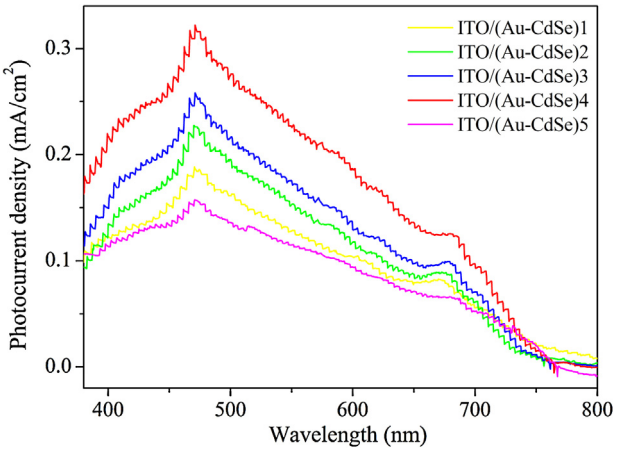

Fig. 10. Wavelength dependent photocurrent response of ITO/(Au–CdSe)$_n$ composite systems (n is the number of Au–CdSe bilayer, typically n = 1–5). The electrodeposition times of gold and CdSe monolayers were 300 s and 9 min, respectively.

of gold NPs within the multilayered film (Fig. 9a). Since the secondary gold NPs are low-density, which gives little contribution to the absorption increase of ITO/(Au–CdSe)$_1$–Au. Therefore, the scattering effect from secondary gold NPs could be weak, and the dramatic absorption enhancement in the ITO/(Au–CdSe)$_2$ should come from the near-field coupling enhancement of plasmonic gold with the adjacent CdSe layers. A similarly observation for the SP broadening and redshift for assembled multilayered Au–TiO_2 film has been reported due to the coupled plasmon interactions of gold NPs in close proximity within the adjacent layers [66]. The Raman experimental results also confirm a stronger Raman scattering of ITO/(Au–CdSe)$_1$–Au than that of the ITO/(Au–CdSe)$_1$ when the secondary gold deposited on the ITO/(Au–CdSe)$_1$ surface (Fig. 9b). This means that the stronger electric fields can be attained from the ITO/(Au–CdSe)$_1$–Au and ITO/(Au–CdSe)$_2$ structures due to the near-field coupling between gold NPs and ambient CdSe layer. Therefore, the absorption of the multilayered Au–CdSe films is also enhanced by the strong local near-field coupling induced by the gold NPs, which is consistent with Yang's simulated results for the polymer tandem solar cell [19]. Besides, we observe an obvious photocurrent density increase with the number of bilayers up to 4 and dramatic decrease of photovoltaic characteristics for the ITO/(Au–CdSe)$_5$ system (Fig. 9c and d). This is possibly due to the limited diffusion of Na_2S into the ITO/(Au–CdSe)$_5$ hybrid electrode with decreased porous ratio and increased thickness. The presence of thick absorber layers would thus impose a high barrier for electron tunneling and transferring between multilayered structures because electron tunneling probability exponentially decays with distance [67]. The broadband photocurrent enhancement of ITO/(Au–CdSe)$_n$ composite systems in the visible light range and the local current maximum between 650 and 700 nm (Fig. 10) suggest the cooperative action of antenna effects and LSP excitation of gold. Our observation in the present paper features the importance of layer-by-layer assembly, which affords the precise control over the architecture of photoanode in achieving the optimum performance *via* simple electrode fabrication technique.

4. Conclusions

We develop porous CdSe photoanodes with effectively enhanced photovoltaic performance by using plasmonic gold nanocrystals as light concentrators. The light scattering and trapping of plasmonic gold nanostructures and the near-field coupling of plasmonic gold with the CdSe semiconductor increase the effective path length of incident light in absorber layer and the absorption of semiconductor surrounding and cross-section, permitting the shrinkage of absorber layer thickness. The gold plasmons also facilitate electron extraction in CdSe semiconductors not only by antenna effects but also by electromagnetic field enhancement due to the localized surface plasmon excitation, resulting in a broadband photocurrent enhancement of composite systems in the visible light range and the local current maximum between 600 and 700 nm. An optimized multilayered Au–CdSe structure shows the predominance in transporting the photogenerated electrons toward the electrode surface to inhibit charge recombination as evidenced increase in photocurrent and open-circuit voltage. The plasmonic light-trapping concept favors new designs for quantum dots-sensitized film solar cells and related energy conversion devices.

Acknowledgements

This work was supported by the National Natural Science Foundation of China (51272237, 61205158, 51272235 and 51172208), the Visiting Scholars Fund of State Key Lab of Silicon Materials, Zhejiang University (SKL2011-20), the Qianjiang Talent Program of Zhejiang Province (QJD1102007), the Excellent Young Talents Foundation of Key Laboratory of Advanced Textile Materials and Manufacturing Technology (Zhejiang Sci-Tech University) (2011QN05), the Young Researchers Foundation of Zhejiang Provincial Top Key Academic Discipline of Applied Chemistry and Eco-Dyeing & Finishing Engineering (ZYG2012005), the Scientific Research Foundation for the Returned Overseas Chinese Scholars (State Education Ministry) and the Technology Foundation for Selected Overseas Chinese Scholar of China.

References

[1] M.A. Green, Recent developments in photovoltaics, Solar Energy 76 (2004) 3.
[2] W.L. Barnes, A. Dereux, T.W. Ebbesen, Surface plasmon subwavelength optics, Nature 424 (2003) 824.
[3] P.A. Mistark, S. Park, S.E. Yalcin, D.H. Lee, O. Yavuzcetin, M.T. Tuominen, T.P. Russell, M. Achermann, Block-copolymer-based plasmonic nanostructures, ACS Nano 3 (2009) 3987.
[4] H.A. Atwater, A. Polman, Plasmonics for improved photovoltaic devices, Nature Materials 9 (2010) 205.
[5] S.K. Cushing, J.T. Li, F.K. Meng, T.R. Senty, S. Suri, M.J. Zhi, M. Li, A.D. Bristow, N.Q. Wu, Photocatalytic activity enhanced by plasmonic resonant energy transfer from metal to semiconductor, Journal of the American Chemical Society 134 (2012) 15033.
[6] D.B. Ingram, S. Linic, Water splitting on composite plasmonic-metal/semiconductor photoelectrodes: Evidence for selective plasmon-induced formation of charge carriers near the semiconductor surface, Journal of the American Chemical Society 133 (2011) 5202.
[7] X.M. Feng, F.X. Ruan, R.J. Hong, J.S. Ye, J.Q. Hu, G.Q. Hu, Z.L. Yang, Synthetically directed self-assembly and enhanced surface-enhanced Raman scattering property of twinned crystalline Ag/Ag homojunction nanoparticles, Langmuir 27 (2011) 2204.
[8] M. Rycenga, C.M. Cobley, J. Zeng, W.Y. Li, C.H. Moran, Q. Zhang, D. Qin, Y.N. Xia, Controlling the synthesis and assembly of silver nanostructures for plasmonic applications, Chemical Reviews 111 (2011) 3669.
[9] S.D. Standridge, G.C. Schatz, J.T. Hupp, Distance dependence of plasmon-enhanced photocurrent in dye-sensitized solar cells, Journal of the American Chemical Society 131 (2009) 8407.
[10] K. Drozdowicz-Tomsia, H. Baltar, E.M. Goldys, Dense two-dimensional silver single and double nanoparticle arrays with plasmonic response in wide spectral range, Langmuir 28 (2012) 9071.
[11] J.F. Zhu, M. Xue, R. Hoekstra, F.X. Xiu, B.Q. Zeng, K.L. Wang, Light concentration and redistribution in polymer solar cells by plasmonic nanoparticles, Nanoscale 4 (2012) 1978.
[12] A.J. Morfa, K.L. Rowlen, T.H. Reilly, M.J. Romero, J. van de Lagemaat, Plasmon-enhanced solar energy conversion in organic bulk heterojunction photovoltaics, Applied Physics Letters 92 (2008) 013504.
[13] J.A. Schuller, E.S. Barnard, W.S. Cai, Y.C. Jun, J.S. White, M.L. Brongersma, Plasmonics for extreme light concentration and manipulation, Nature Materials 9 (2010) 193.
[14] R.A. Pala, J. White, E. Barnard, J. Liu, M.L. Brongersma, Design of plasmonic thin-film solar cells with broadband absorption enhancements, Advanced Materials 21 (2009) 3504.

[15] P. Muhlschlegel, H.J. Eisler, O.J.F. Martin, B. Hecht, D.W. Pohl, Resonant optical antennas, Science 308 (2005) 1607.
[16] N.C. Jeong, C. Prasittichai, J.T. Hupp, Photocurrent enhancement by surface plasmon resonance of silver nanoparticles in highly porous dye-sensitized solar cells, Langmuir 27 (2011) 14609.
[17] M.D. Brown, T. Suteewong, R.S.S. Kumar, V. D'Innocenzo, A. Petrozza, M.M. Lee, U. Wiesner, H.J. Snaith, Plasmonic dye-sensitized solar cells using core-shell metal-insulator nanoparticles, Nano Letters 11 (2011) 438.
[18] T. Kawawaki, Y. Takahashi, T. Tatsuma, Enhancement of dye-sensitized photocurrents by gold nanoparticles: effects of dye-particle spacing, Nanoscale 3 (2011) 2865.
[19] J. Yang, J.B. You, C.C. Chen, W.C. Hsu, H.R. Tan, X.W. Zhang, Z.R. Hong, Y. Yang, Plasmonic polymer tandem solar cell, ACS Nano 5 (2011) 6210.
[20] D.H. Wang, D.Y. Kim, K.W. Choi, J.H. Seo, S.H. Im, J.H. Park, O.O. Park, A.J. Heeger, Enhancement of donor-acceptor polymer bulk heterojunction solar cell power conversion efficiencies by addition of Au nanoparticles, Angewandte Chemie International Edition 50 (2011) 5519.
[21] D.D.S. Fung, L.F. Qiao, W.C.H. Choy, C.D. Wang, W.E.I. Sha, F.X. Xie, S.L. He, Optical and electrical properties of efficiency enhanced polymer solar cells with Au nanoparticles in a PEDOT-PSS layer, Journal of Materials Chemistry 21 (2011) 16349.
[22] C.C.D. Wang, W.C.H. Choy, C.H. Duan, D.D.S. Fung, W.E.I. Sha, F.X. Xie, F. Huang, Y. Cao, Optical and electrical effects of gold nanoparticles in the active layer of polymer solar cells, Journal of Materials Chemistry 22 (2012) 1206.
[23] A.P. Kulkarni, K.M. Noone, K. Munechika, S.R. Guyer, D.S. Ginger, Plasmon-enhanced charge carrier generation in organic photovoltaic films using silver nanoprisms, Nano Letters 10 (2010) 1501.
[24] J. Du, J. Qi, D. Wang, Z.Y. Tang, Facile synthesis of Au@TiO2 core-shell hollow spheres for dye-sensitized solar cells with remarkably improved efficiency, Energy & Environmental Science 5 (2012) 6914.
[25] K. Awazu, M. Fujimaki, C. Rockstuhl, J. Tominaga, H. Murakami, Y. Ohki, N. Yoshida, T. Watanabe, A plasmonic photocatalyst consisting of sliver nanoparticles embedded in titanium dioxide, Journal of the American Chemical Society 130 (2008) 1676.
[26] E. Thimsen, F. Le Formal, M. Gratzel, S.C. Warren, Influence of plasmonic Au nanoparticles on the photoactivity of Fe2O3 electrodes for water splitting, Nano Letters 11 (2011) 35.
[27] Z.W. Liu, W.B. Hou, P. Pavaskar, M. Aykol, S.B. Cronin, Plasmon resonant enhancement of photocatalytic water splitting under visible illumination, Nano Letters 11 (2011) 1111.
[28] H. Wang, T.T. You, W.W. Shi, J.H. Li, L. Guo, Au/TiO2/Au as a plasmonic coupling photocatalyst, Journal of Physical Chemistry C 116 (2012) 6490.
[29] P. Chatchai, S.Y. Kishioka, Y. Murakami, A.Y. Nosaka, Y. Nosaka, Enhanced photoelectrocatalytic activity of FTO/WO3/BiVO4 electrode modified with gold nanoparticles for water oxidation under visible light irradiation, Electrochimica Acta 55 (2010) 592.
[30] S.E. Lee, L.P. Lee, Biomolecular plasmonics for quantitative biology and nanomedicine, Current Opinion in Biotechnology 21 (2010) 489.
[31] F. Xiao, J.B. Song, H.C. Gao, X.L. Zan, R. Xu, H.W. Duan, ACS Coating graphene paper with 2D-assembly of electrocatalytic nanoparticles: A modular approach toward high-performance flexible electrodes, ACS Nano 6 (2012) 100.
[32] A.P. Liu, T. Xu, Q.H. Ren, M. Yuan, W.J. Dong, W.H. Tang, Graphene modulated 2D assembly of plasmonic gold nanostructure on diamond-like carbon substrate for surface-enhanced Raman scattering, Electrochemistry Communications 25 (2012) 74.
[33] J.W. Menezes, J. Ferreira, M.J.L. Santos, L. Cescato, A.G. Brolo, Large-area fabrication of periodic arrays of nanoholes in metal films and their application in biosensing and plasmonic-enhanced photovoltaics, Advanced Functional Materials 20 (2010) 3918.
[34] G. Lu, H. Li, S.X. Wu, P. Chen, H. Zhang, High-density metallic nanogaps fabricated on solid substrates used for surface enhanced Raman scattering, Nanoscale 4 (2012) 860.
[35] K.L. Kelly, E. Coronado, L.L. Zhao, G.C. Schatz, The optical properties of metal nanoparticles: The influence of size, shape, and dielectric environment, Journal of Physical Chemistry B 107 (2003) 668.
[36] X.H. Li, W.C.H. Choy, L.J. Huo, F.X. Xie, W.E.I. Sha, B.F. Ding, X. Guo, Y.F. Li, J.H. Hou, J.B. You, Y. Yang, Dual plasmonic nanostructures for high performance inverted organic solar cells, Advanced Materials 24 (2012) 3046.
[37] H. Wei, F. Hao, Y.Z. Huang, W.Z. Wang, P. Nordlander, H.X. Xu, Polarization dependence of surface-enhanced Raman scattering in gold nanoparticle-nanowire systems, Nano Letters 8 (2008) 2497.
[38] U. Dogan, M. Kaya, A. Cihaner, M. Volkan, Ag nanostructures on a poly(3,4-ethylenedioxythiophene) film prepared with electrochemical route: A controllable roughened SERS substrate with high repeatability and stability, Electrochimica Acta 85 (2012) 220.
[39] J.X. Fang, H.J. You, B.J. Ding, X.P. Song, Large-area and high-density gold nanoparticle arrays with sub-10 nm gaps, Electrochemistry Communications 9 (2007) 2423.
[40] A.P. Liu, Q.H. Ren, T. Xu, M. Yuan, W.H. Tang, Morphology-controllable gold nanostructures on phosphorus doped diamond-like carbon surfaces and their electrocatalysis for glucose oxidation, Sensors and Actuators B: Chemical 162 (2012) 135.
[41] Y. Tian, T. Tatsuma, Mechanisms and applications of plasmon-induced charge separation at TiO_2 films loaded with gold nanoparticles, Journal of the American Chemical Society 127 (2005) 7632.
[42] L. Cheng, A.P. Liu, S. Peng, H.W. Duan, Responsive plasmonic assemblies of amphiphilic nanocrystals at oil-water interfaces, ACS Nano 4 (2010) 6098.
[43] B.M. Reinhard, M. Siu, H. Agarwal, A.P. Alivisatos, J. Liphardt, Calibration of dynamic molecular rule based on plasmon coupling between gold nanoparticles, Nano Letters 5 (2005) 2246.
[44] I. Bannat, K. Wessels, T. Oekermann, J. Rathousky, D. Bahnemann, M. Wark, Improving the photocatalytic performance of mesoporous titania films by modification with gold nanostructures, Chemistry of Materials 21 (2009) 1645.
[45] P. Reineck, G.P. Lee, D. Brick, M. Karg, P. Mulvaney, U. Bach, A solid-state plasmonic solar cell via metal nanoparticle self-assembly, Advanced Materials 24 (2012) 4750.
[46] E. Kazuma, N. Sakai, T. Tatsuma, Nanoimaging of localized plasmon-induced charge separation, Chemical Communications 47 (2011) 5777.
[47] M. Heo, H. Cho, J.W. Jung, J.R. Jeong, S. Park, J.Y. Kim, High-performance organic optoelectronic devices enhanced by surface plasmon resonance, Advanced Materials 23 (2011) 5689.
[48] N. Shpaisman, U. Givan, F. Patolsky, Electrochemical synthesis of morphology-controlled segmented CdSe nanowires, ACS Nano 4 (2010) 1901.
[49] A.M. Kressin, V.V. Doan, J.D. Klein, M.J. Sailor, Synthesis of stoichiometric cadmium selenide films via sequential monolayer electrodeposition, Chemistry of Materials 3 (1991) 1015.
[50] R. Henriquez, A. Badan, P. Grez, E. Munoz, J. Vera, E.A. Dalchiele, R.E. Marotti, H. Gomez, Electrodeposition of nanocrystalline CdSe thin films from dimethyl sulfoxide solution: Nucleation and growth mechanism, structural and optical studies, Electrochimica Acta 56 (2011) 4895.
[51] P. Bocchetta, M. Santamaria, F.D. Quarto, One-step electrochemical synthesis and physico-chemical characterization of CdSe nanotubes, Electrochimica Acta 88 (2013) 340.
[52] E.B. Chubenko, A.A. Klyshko, V.A. Petrovich, V.P. Bondarenko, Electrochemical deposition of zinc selenide and cadmium selenide onto porous silicon from aqueous acidic solutions, Thin Solid Films 517 (2009) 5981.
[53] M. Skyllas Kazcos, B. Miller, Studies in selenious acid reduction and CdSe film deposition, Journal of the Electrochemical Society 127 (1980) 869.
[54] S.M. Pawar, A.V. Moholkar, C.H. Bhosale, Influence of pH on electrochemically deposited CdSe thin films, Materials Letters 61 (2007) 1034.
[55] Z.F. Feng, Q.B. Zhang, L.L. Lin, H.H. Quo, J.Z. Zhou, Z.H. Lin, ⟨0 0 0 1⟩-preferential growth of CdSe nanowires on conducting glass: Template-free electrodeposition and application in photovoltaics, Chemistry of Materials 22 (2010) 2705.
[56] J.B. Zhang, Y. Lin, X.R. Xiao, R.Z. Wang, Characterization of nanocrystalline porous CdSe thin films by electrolyte electroabsorption spectroscopy, Thin Solid Films 479 (2005) 188.
[57] D.M. Schaadt, B. Feng, E.T. Yu, Enhanced semiconductor optical absorption via surface plasmon excitation in metal nanoparticles, Applied Physics Letters 86 (2005) 063106.
[58] S.S. Kim, S.I. Na, J. Jo, D.Y. Kim, Y.C. Nah, Plasmon enhanced performance of organic solar cells using electrodeposited Ag nanoparticles, Applied Physics Letters 93 (2008) 073307.
[59] J.L. Wu, F.C. Chen, Y.S. Hsiao, F.C. Chien, P.L. Chen, C.H. Kuo, M.H. Huang, C.S. Hsu, Surface plasmonic effects of metallic nanoparticles on the performance of polymer bulk heterojunction solar cells, ACS Nano 5 (2011) 959.
[60] R. Bukasov, T.A. Ali, P. Nordlander, J.S. Shumaker-Parry, Probing the plasmonic near-field of gold nanocrescent antennas, ACS Nano 4 (2010) 6639.
[61] J.F. Zhu, M. Xue, H.J. Shen, Z. Wu, S. Kim, J.J. Ho, A. Hassani-Afshar, B.Q. Zeng, K.L. Wang, Plasmonic effects for light concentration in organic photovoltaic thin films induced by hexagonal periodic metallic nanospheres, Applied Physics Letters 98 (2011) 151110.
[62] K.A. Willets, R.P. Van Duyne, Localized surface plasmon resonance spectroscopy and sensing, Annual Review of Physical Chemistry 58 (2007) 267.
[63] A.K. Arora, A.K. Ramdas, Resonance Raman-scattering from defects in CdSe, Physical Review B 35 (1987) 4345.
[64] D. Pacifici, H.J. Lezec, H.A. Atwater, All-optical modulation by plasmonic excitation of CdSe quantum dots, Nature Photonics 1 (2007) 402.
[65] Y. Takahashi, S. Taura, T. Akiyama, S. Yamada, Electropolymerized polythiophene photoelectrodes with density-controlled gold nanoparticles, Langmuir 28 (2012) 9155.
[66] W.Y. Yuan, C.M. Li, Direct modulation of localized surface plasmon coupling of Au nanoparticles on solid substrates via weak polyelectrolyte-mediated layer-by-layer self assembly, Langmuir 25 (2009) 7578.
[67] M. Kondon, J. Kim, N. Udawatte, D. Lee, Origin of size-dependent energy transfer from photoexcited CdSe quantum dots to gold nanoparticles, Journal of Physical Chemistry C 112 (2008) 6695.